Journal of Engineering Science *Vol. XXXII, no. 4 (2025), pp. 7 - 18*
Fascicle *Industrial Engineering* *ISSN 2587-3474*
Topic *Materials Science and New Technologies* *eISSN 2587-3482*

https://doi.org/10.52326/jes.utm.2025.32(4).01.
UDC 537.32:538.9:539.21

TTT_2I_3 ORGANIC CRYSTALS – A PROMISING PLATFORM FOR LOW-DIMENSIONAL THERMOELECTRIC DEVICES

Silvia Andronic *, ORCID: 0000-0002-7092-6867,
Ionel Sanduleac, ORCID: 0000-0001-7532-1288

Technical University of Moldova, 168 Stefan cel Mare Blvd, Chisinau, Republic of Moldova
* Corresponding author: Silvia Andronic, *silvia.andronic@mt.utm.md*

Received: 12. 02. 2025
Accepted: 12. 28. 2025

Abstract. In this paper, we provide an analysis of quasi-one-dimensional organic crystals of TTT_2I_3 (tetrathiotetracene-iodide) with respect to their thermoelectric properties. An advanced physical model was employed. The main Hamiltonian of the model includes the electronic and phonon contributions, electron-phonon interactions, and an impurity-scattering term. To capture charge transport between molecular chains, the model was extended to a three-dimensional framework. Numerical simulations were conducted to evaluate electrical conductivity, Seebeck coefficient, thermal conductivity, thermoelectric power factor, and figure of merit as functions of carrier concentration, temperature, and impurity content. Additionally, the Peierls structural transition in the TTT chains was analyzed, allowing determination of the critical transition temperature. The dispersion of renormalized phonons was examined in the random phase approximation for different temperatures.

Keywords: *carrier concentration, electron-phonon interaction, organic materials, Peierls critical temperature, power factor, renormalized phonon spectrum, Seebeck coefficient, thermal conductivity.*

Rezumat. În această lucrare, prezentăm o analiză a cristalelor organice cvasi-unidimensionale de TTT_2I_3 (tetratiotetracen-iodid) din perspectiva proprietăților lor termolectrice. A fost utilizat un model fizic avansat. Hamiltonianul principal al modelului include contribuțiile electronice și fononice, interacțiunile electron - fonon și un termen asociat împrăștierii pe impurități. Pentru a descrie transportul de sarcină între lanțurile moleculare, modelul a fost extins la un cadru tridimensional. Au fost efectuate simulări numerice pentru a determina conductivitatea electrică, coeficientul Seebeck, conductivitatea termică, factorul de putere termolectric și parametrul termolectric de calitate în funcție de concentrația purtătorilor de sarcină, temperatură și conținutul de impurități. De asemenea, a fost analizată tranziția structurală de tip Peierls în lanțurile TTT, ceea ce a permis determinarea temperaturii critice a tranziției. Dispersia fononilor renormați a fost examinată în aproximația fazelor aleatorii pentru diferite temperaturi.

Cuvinte cheie: *concentrația purtătorilor de sarcină, interacțiune electron-fonon, materiale organice, temperatura critică Peierls, factor de putere, spectrul renormalizat al fononilor, coeficient Seebeck, conductivitatea termică.*

1. Introduction

A significant portion of global energy is currently produced using fossil-fuel heat engines, whose limited efficiency results in substantial waste heat. Developing cost-effective methods to convert part of this unused thermal energy into electricity has therefore become an important technological objective. Thermoelectric generators represent a promising solution, as they enable direct heat-to-electricity conversion and can also operate as solid-state refrigeration devices without mechanical components.

The dimensionless thermoelectric figure of merit, $ZT = \sigma S^2 T k^{-1}$, is the primary parameter determining a material's suitability for thermoelectric energy conversion. Here, σ is the electrical conductivity, S the Seebeck coefficient, $k = k^e + k^L$ the total thermal conductivity including electronic (k^e) and lattice (k^L) contributions, and T the operating temperature. Achieving high ZT values is essential for efficient energy conversion, yet these parameters are interdependent: increasing σ can reduce S and increase k^e, making the simultaneous optimization of all factors challenging. In recent decades, significant progress has been made, particularly in low-dimensional inorganic structures. High ZT values, such as ~2.4 has been measured [1] at room temperature in *p*-type Bi_2Te_3/Sb_2Te_3 superlattices. ZT ~ 3 has been reported in PbTeSe quantum dot superlattices [2], and even ZT ~ 3.5 [3,4] have been reported. However, these materials typically involve complex and costly fabrication processes, and commercially available Bi_2Te_3-based thermoelectrics currently reach ZT ~1 around 500 K. Attaining ZT >3 would make solid-state thermoelectric devices economically competitive with conventional energy conversion technologies, but large-scale commercialization remains limited. Despite these challenges, miniaturized thermoelectric modules are already mass-produced for practical applications, including temperature stabilization in laser diodes [5], climate-controlled automotive seats [6], portable coolers [7], and space technologies. Recent strategies for scaling up production suggest combining high-energy ball milling with aerosol jet printing to produce devices with high electrical conductivity and low thermal conductivity, resulting in a maximized ZT. This approach highlights the ongoing potential of thermoelectric materials for energy harvesting and refrigeration applications [8-10]. A detailed review of thermoelectric materials and their applications was presented in [11].

Organic compounds have recently gained attention due to their cost-effectiveness, abundance, environmental friendliness, and unique properties. Examples include poly(3,4-ethylenedioxythiophene) (PEDOT) doped with poly(styrenesulphonate) (PSS), where thin films of *p*-type have registered a ZT value of 0.42 at room temperature [12]. Even higher ZT values, reaching around 1, have been reported in films of PP-PEDOT/Tos [13]. Such results underline the opportunities offered by organic materials for next-generation thermoelectric devices.

High ZT values have been predicted in certain quasi-one-dimensional (Q1D) organic crystals, such as TTT_2I_3 [14] and $TTT(TCNQ)_2$ [15]. These materials consist of linear molecular chains or stacks within a three-dimensional lattice, with interactions along the chains dominating over interchain interactions. Many organic compounds, including ion-radical salts like TTF-TCNQ, crystalline polymers, and specific charge transfer complexes, exhibit this

quasi-one-dimensional structure, which often leads to unique properties. Previous predictions of high *ZT* were based on simplified one-dimensional models. In existing Q1D crystals of tetrathiotetracene-iodide, TTT_2I_3, grown from solution [16] with measured electrical conductivity $\sigma_{xx} = 1.8 \cdot 10^5\, \Omega^{-1} m^{-1}$, Seebeck coefficient $S_{xx} = 39\, \mu V K^{-1}$ and thermal conductivity $k_{xx} = 1.0 W m^{-1} K^{-1}$ along the conductive chains only *ZT* ≅ 0.1 was obtained at room temperature [17]. Such low value of *ZT* is explained by the fact that the crystals were not very pure and the parameters were not optimized. We have developed a more realistic three-dimensional model, enabling more accurate simulations of the thermoelectric behavior of selected Q1D organic crystals.

The objective of this paper is to present the results of recent investigations on quasi-one-dimensional (Q1D) organic crystals and their potential applications in thermoelectric systems. The study provides a comprehensive analysis, including modeling and evaluation of key properties such as electrical conductivity, Seebeck coefficient, thermal conductivity, thermoelectric power factor and the thermoelectric figure of merit. Additionally, the research examines the Peierls structural transition in the TTT molecular chains of TTT_2I_3, determining the critical transition temperature and analyzing the dispersion of renormalized phonons across different temperatures and dimensionless Fermi momentum (k_F) values.

2. Three-Dimensional Physical Model of the Crystal

The Q1D crystals of TTT_2I_3 are formed from segregate stacks or chains of TTT molecules and iodine. However, only the TTT chains are conductive, owing to the strong π-electron overlap along their stacks. Each pair of TTT molecules donates one electron to the iodine chain composed of I_3^- ions, which act as electron acceptors. The electrons on the I_3^- ions are strongly localized and therefore do not contribute to charge transport. As a result, the carriers are holes. The electrical conductivity along the TTT chains is nearly three orders of magnitude higher than in the transverse directions. In earlier studies, this pronounced anisotropy justified the use of a simplified 1D model [18,19], where the crystal was regarded as consisting of independent one-dimensional chains arranged in a 3D crystal framework. In reality, the 1D conductive chains are not completely independent, as weak interchain interactions are present. It is evident that this interchain interaction affects the validity of the 1D approximation - most notably in very pure crystals, where it restricts the mobility of charge carriers. Therefore, it is crucial to determine how interchain interactions influence the thermoelectric properties of real crystals and, in this context, to establish the conditions under which the simpler 1D model remains applicable.

In this Section we will present the physical model of the TTT_2I_3 crystal that was described in more detail in [20]. The Hamiltonian of the 3D crystal model was formulated using the tight-binding approach and the nearest-neighbor approximation. It can be expressed as follows:

$$H = \sum_{\boldsymbol{k}} \varepsilon(\boldsymbol{k}) a_{\boldsymbol{k}}^{+} a_{\boldsymbol{k}} + \sum_{\boldsymbol{q}} \hbar \omega_{\boldsymbol{q}} b_{\boldsymbol{q}}^{+} b_{\boldsymbol{q}} + \sum_{\boldsymbol{k},\boldsymbol{q}} A(\boldsymbol{k},\boldsymbol{q}) a_{\boldsymbol{k}}^{+} a_{\boldsymbol{k}-\boldsymbol{q}} (b_{\boldsymbol{q}} + b_{-\boldsymbol{q}}^{+}). \quad (1)$$

The first term in Eq. (1), $\sum_{\boldsymbol{k}} \varepsilon(\boldsymbol{k}) a_{\boldsymbol{k}}^{+} a_{\boldsymbol{k}}$, represents the energy operator of free electrons in the periodic field of the lattice. The second term, $\sum_{\boldsymbol{q}} \hbar \omega_{\boldsymbol{q}} b_{\boldsymbol{q}}^{+} b_{\boldsymbol{q}}$, corresponds to the energy

operator of longitudinal acoustic phonons. The third term, $\sum_{\boldsymbol{k},\boldsymbol{q}} A(\boldsymbol{k},\boldsymbol{q}) a_{\boldsymbol{k}}^{+} a_{\boldsymbol{k}-\boldsymbol{q}} (b_{\boldsymbol{q}} + b_{-\boldsymbol{q}}^{+})$ describes the two most significant electron-phonon interactions. Here, $\varepsilon(\boldsymbol{k})$ represents the carrier energy, where $a_{\boldsymbol{k}}^{+}, a_{\boldsymbol{k}}$ are the electron creation and annihilation operators associated with the 3D quasi-wave vector $\boldsymbol{k}$ (k_x, k_y, k_z). Analogously, b_q^{+}, b_q denote the acoustic phonon creation and annihilation operators for a 3D wave vector $\boldsymbol{q}$ and frequency $\omega_{\boldsymbol{q}}$. The interaction matrix element is given by $A(\boldsymbol{k},\boldsymbol{q})$. The electron energy $\varepsilon(\boldsymbol{k})$, measured relative to the top of the band, takes the following form:

$$\varepsilon(\boldsymbol{k}) = -2w_1(1-\cos k_x b) - 2w_2(1-\cos k_y a) - 2w_3(1-\cos k_z c), \tag{2}$$

where: w_1, w_2 and w_3 are the transfer energies of a hole along the chain *(x* direction) and perpendicular to it (*y* and *z* directions), respectively.

It is established that the Peierls transition happens at low temperatures. Consequently, the interaction of electrons with optical phonons can be ignored, and the acoustic phonon spectrum of a simple one-dimensional chain can be represented by [21]:

$$\omega_{\boldsymbol{q}}^2 = \omega_1^2 \sin^2(q_x b/2) + \omega_2^2 \sin^2(q_y a/2) + \omega_3^2 \sin^2(q_z c/2). \tag{3}$$

In Eq. (3) the limit frequencies in the *x*, *y*, and *z* directions are denoted by ω_1, ω_2 and ω_3, respectively. In this model, two hole – phonon interactions are considered. The first has coupling constants proportional to the derivatives w_1', w_2' and w_3' of w_1, w_2, and w_3 with respect to intermolecular distances, while the second depends on the molecule's average polarizability α_0. The latter is especially important for crystals of large molecules, such as TTT, since α_0 scales approximately with molecular volume.

The square module of matrix element $A(\boldsymbol{k},\boldsymbol{q})$ from Eq. (1) has the following form:

$$\begin{aligned} |A(\boldsymbol{k},\boldsymbol{q})|^2 = {} & 2\hbar w_1'^2 / (NM\omega_{\boldsymbol{q}}) \Big\{ \Big[\sin(k_x b) - \sin(k_x - q_x, b) - \gamma_1 \sin(q_x b) \Big]^2 + \\ & + d_1^2 \Big[\sin(k_y a) - \sin(k_y - q_y, a) - \gamma_2 \sin(q_y a) \Big]^2 + \\ & + d_2^2 \Big[\sin(k_z c) - \sin(k_z - q_z, c) - \gamma_3 \sin(q_z c) \Big]^2 \Big\}. \end{aligned} \tag{4}$$

In Eq. (4), *M* denotes the mass of a TCNQ molecule, and *N* represents the number of TCNQ molecules in the basic region of the crystal; $d_1 = w_2 / w_1 = w_2' / w_1'$; $d_2 = w_3 / w_1 = w_3' / w_1'$; parameters γ_1, γ_2 and γ_3 correspond to the ratio of the polaron - type interaction amplitude to the deformation potential in the *x*, *y*, and *z* directions, respectively.

$$\gamma_1 = 2e^2\alpha_0 / b^5 w_1'; \;\; \gamma_2 = 2e^2\alpha_0 / a^5 w_2'; \;\; \gamma_3 = 2e^2\alpha_0 / c^5 w_3'. \tag{5}$$

The analysis indicates that the Hamiltonian from Eq. (1) cannot account for the sharp decrease in electrical conductivity observed at temperatures below $T_{max} = 35\ K$, even when varying crystal parameters and considering only the first interaction mechanism. It is therefore necessary to include the dynamic interaction of carriers with defects. The static interaction contributes to the renormalization of the hole spectrum. In TTT_2I_3 crystals, defects

arise due to the different thermal expansion coefficients of the TTT and iodine chains. The Hamiltonian describing this interaction is expressed as follows:

$$H_{def} = \sum_{\boldsymbol{k},\boldsymbol{q}} \sum_{n=1}^{N_d} B(q_x) \exp(-iq_x x_n) a_k^+ a_{k-q} (b_q + b_q^-). \tag{6}$$

In Eq. (6), the variable x_n indexes the defects, which are assumed to be linear along the *x* - direction of the TTT chains and randomly distributed. $B(q_x)$ represents the matrix element describing the interaction of a hole with a defect, and is given by the following expression:

$$B(q_x) = \sqrt{\hbar / (2NM\omega_q)} \cdot I(q_x), \tag{7}$$

where: $I(q_x)$ is the Fourier transformation of the derivative of the carrier–defect interaction energy with respect to the intermolecular distance.

$$I(q_x) = D(\sin(bq_x))^2. \tag{8}$$

In this context, *D* characterizes the strength of the hole–defect coupling, equivalent to w_1' in Eq. (5), and the Peierls transition is strongly influenced by its value.

The renormalized phonon spectrum $\Omega(q)$ is obtained from the pole of the Green function, which is defined by the transcendent dispersion equation.

$$\Omega(q) = \omega_q [1 - \bar{\Pi}(q, \Omega)]^{1/2}, \tag{9}$$

where the principal value of the dimensionless polarization operator is given by

$$\mathrm{Re}\,\bar{\Pi}(q,\Omega) = -\frac{4}{\hbar\omega_q} \sum_{\boldsymbol{k}} \frac{[|A(\boldsymbol{k},-\boldsymbol{q})|^2 + |B(\boldsymbol{q}_x)|^2](n_{\boldsymbol{k}} - n_{\boldsymbol{k}+\boldsymbol{q}})}{\varepsilon(\boldsymbol{k}) - \varepsilon(\boldsymbol{k}+\boldsymbol{q}) + \hbar\Omega}. \tag{10}$$

$n_{\boldsymbol{k}}$ represents the Fermi distribution function. We note, that Eq. (9) is solvable exclusively by numerical methods.

Transport properties. Consider the case in which a weak electric field and a small temperature gradient are imposed along the conductive chains. At room temperature, the phonon energy and the transversal kinetic energy of the holes can be neglected in the scattering processes, as both are much smaller than the kinetic energy associated with motion along the chains. Under these conditions, the linearized kinetic equation can be solved analytically, allowing the electrical conductivity σ_{xx}, the Seebeck coefficient S_{xx}, the electronic thermal conductivity k_{xx}^e and the thermoelectric figure of merit $(ZT)_{xx}$ to be expressed in terms of the transport integrals R_n as follows:

$$\sigma_{xx} = \sigma_0 R_0,\ S_{xx} = (k_0 / e)(2w_1 / k_0 T) R_1 / R_0, \tag{11}$$

$$k_{xx}^e = [4w_1^2 \sigma_0 / (e^2 T)](R_2 - R_1^2 / R_0),\ (ZT)_{xx} = \sigma_{xx} S_{xx}^2 T / (k_{xx}^L + k_{xx}^e), \tag{12}$$

where

$$\sigma_0 = (2e^2 M v_{s1}^2 w_1^3 r) / (\pi^2 \hbar abc (k_0 T)^2 w_1'^2). \tag{13}$$

Here, $r = 4$ denotes the number of molecular chains present in the transverse cross-section of the unit cell. The term k_{xx}^{L} represents the lattice thermal conductivity, v_{s1} is the sound velocity along the chains, and R_n are the transport integrals.

$$R_n = \int_0^2 d\varepsilon \int_0^{\pi} d\eta \int_0^{\pi} d\varsigma \varepsilon(2-\varepsilon) n_{\varepsilon,\eta,\varsigma}(1-n_{\varepsilon,\eta,\varsigma}) \times \\ \times \frac{[\varepsilon + d_1(1-\cos\eta) + d_2(1-\cos\varsigma) - (1+d_1+d_2)\varepsilon_F]^n}{\gamma_1^2(\varepsilon-\varepsilon_0)^2 + D_0 + \{d_1^2(1+\gamma_2^2+2\sin^2\eta - 2\gamma_2\cos\eta) + d_2^2(1+\gamma_3^2+2\sin^2\varsigma - 2\gamma_3\cos\varsigma)\}/(8\varepsilon(2-\varepsilon))}. \quad (14)$$

For comparison with the 1D model, the following dimensionless variables were introduced:
$\varepsilon = 1-\cos(bk_x)$, $\eta = k_y a$, and $\varsigma = k_z c$. In this representation, $n_{\varepsilon,\eta,\varsigma}$ denotes the Fermi distribution function expressed in terms of the new variables. The dimensionless resonance energy appearing in the relaxation time is given by $\varepsilon_0 = (\gamma_1 - \gamma)/\gamma_1$ and is measured in units of $2w_1$. The parameters $d_1 = w_2/w_1 = w_2'/w_1'$; $d_2 = w_3/w_1 = w_3'/w_1'$; characterize the ratios of the transfer integrals. The 1D Fermi energy is defined as $\varepsilon_F = E_F/(2w_1)$, while the corresponding 3D Fermi energy becomes $2w_1(1+d_1+d_2)\varepsilon_F$. The parameter D_0 quantifies the scattering of holes by impurities.

$$D_0 = n_{im}^{3D} I^2 V_0^2 \frac{Mv_s^2}{4b^3 acw_1'^2 k_0 T}, \quad (15)$$

where: n_{im}^{3D} denotes the impurity density, I represents the amplitude of the impurity potential, and V_0 is the spatial region over which this potential acts.

To determine the parameters d_1 and d_2, the electrical conductivity in the transverse directions, σ_{yy} and σ_{zz}, was calculated. In these directions, the overlap of hole wave functions is minimal, making it convenient to express the system Hamiltonian in the representation of localized states on the TTT molecules. Consequently, for motion along the *y* and *z* axes, the dominant term in the Hamiltonian is the hole - phonon interaction, while the term describing hole motion within the periodic lattice potential is treated as a small perturbation. A canonical transformation is applied to the Hamiltonian, allowing the main contribution of the hole - phonon interaction to be accounted for already at the zero - order approximation. This procedure also results in a substantial narrowing of the original conduction band along the conductive chains. As a result, transport in the transverse directions occurs via a hopping mechanism, with the charge carriers effectively behaving as small polarons.

The expressions for σ_{yy} and σ_{zz} were computed numerically. By comparing these results with the experimental data, $\sigma_{yy} \approx \sigma_{zz} = 3.3\Omega^{-1}cm^{-1}$, it can be inferred that $w_2 = w_3 = 0.015w_1$. The similarity of these values reflects the close correspondence between the lattice constants *a* and *c* along the *y* and *z* directions, respectively.

3. Results and Discussions

Computer simulations were carried out using the following set of parameters [17]: $M = 6.5\times10^5 m_e$ (where m_e is the free-electron mass), $w_1 = 0.16eV$, $w_1' = 0.26eV\cdot Å^{-1}$, $a = 18.35Å$, $b = 4.96Å$, $c = 18.46Å$. The sound velocity at low temperatures along the chains (i.e., in the *b* direction) is $v_{s1} = 1.5\times10^5 cm\cdot s^{-1}$. The parameter d is set to 0.015, while $\gamma_1 = 1.7$ and γ_2 is obtained from the relation $\gamma_2 = \gamma_1 b^5 / a^5 d$. For the transversal sound velocity in the *a* direction, the value $v_{s2} = 1.35\times10^5 cm\cdot s^{-1}$ was used. The dimensionless parameters for describing the impurity scattering were considered as follows: $D_0 = 0.001$ for static impurities and $D_1 = 0.2$ for lattice defects, thermally activated.

First of all, the computer calculations were performed for different values of free parameters in order to adjust the physical model by comparison with experimentally reported data (Figures 1, 2). In Figure 1 the experimental data from [16] were considered for TTT_2I_3 crystals. The measured electrical conductivity along TTT chains at room temperature is $1.8\cdot10^5 \Omega^{-1}m^{-1}$. It can be observed that for temperatures, lower than a threshold, the computer simulations are diverging from experiment. This can be explained by the reshape of crystalline lattice with temperature decrease, a smooth metal-dielectric transition takes place for temperatures below $100\,K$. The three lines represent calculated values for electrical conductivity for three values of dimensionless Fermi energy $\varepsilon_F = 0.27, 0.3, 0.33$. For stoichiometric crystals $\varepsilon_F = 0.37$. It is observed that the theory describes well the temperature dependence of electrical conductivity in the range from $180\,K$ to $400\,K$. It has to be mentioned that electrical conductivity in such crystals is provided by holes, due to the presence of iodine atoms. With the increase of temperature, the iodine evaporates and the physical model is not more applicable.

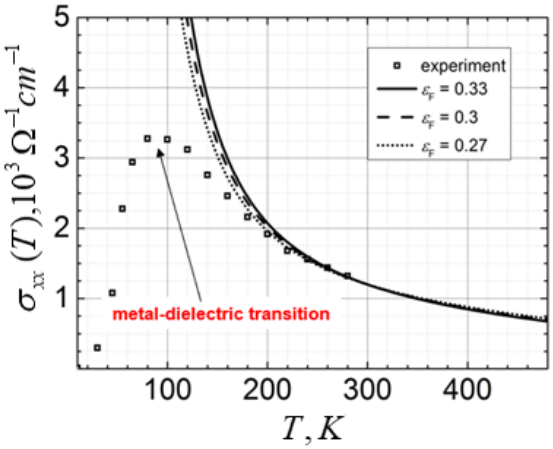

Figure 1. Electrical conductivity as a function of temperature *T*: rhombs – experiment [16]; lines – numerical results.

In Figure 2 the results for thermopower S_{xx} are presented as a function of temperature for different levels of dimensionless Fermi energy. It is observed that in this case the fluctuations of the dielectric phase practically do not affect the behavior of S_{xx} for a wide interval of temperatures. For crystals with near-to stoichiometric concentration of conducting holes (continuous line), the numerical results are fitting the experimentally reported ones. With the decrease of ε_F one can obtain higher values for thermopower, especially for near-to room temperatures, a perspective results for thermoelectric applications.

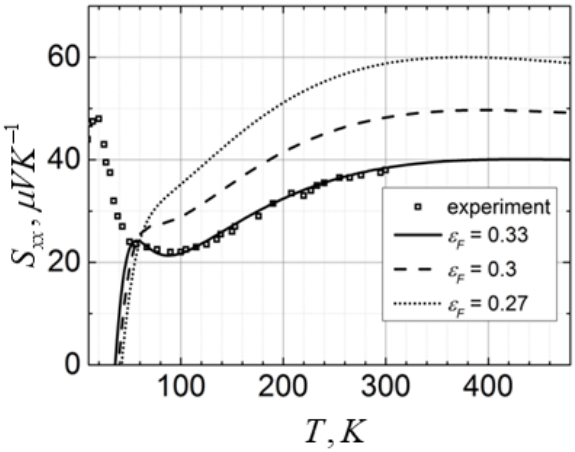

Figure 2. Thermopower as a function of temperature *T*: rhombs – experiment [16]; lines – numerical results.

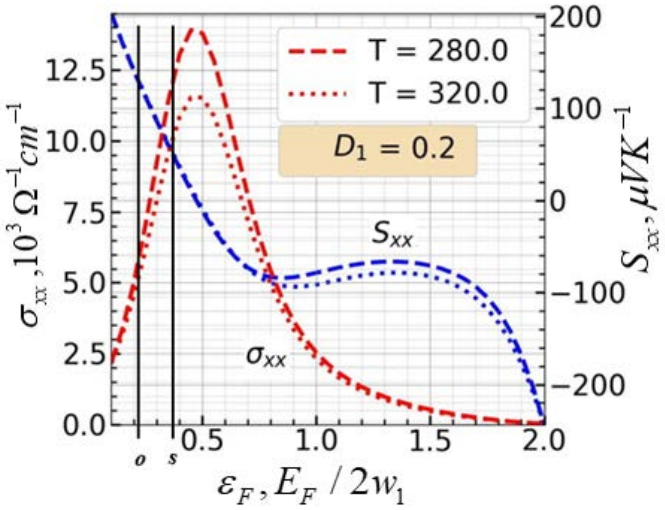

Figure 3. Electrical conductivity and Seebeck coefficient as a function of dimensionless Fermi energy. D_1 – scattering on lattice defects.

Considering that crystals are organic and for temperatures higher than $350-400\,K$ the iodine evaporates, we calculated in detail the electrical conductivity and the thermopower for two values of *T*: $280\,K$ and $320\,K$ for a wide range of dimensionless Fermi energy (Figure 3). It is observed that electrical conductivity is more sensitive to temperature changes, mainly at $\varepsilon_F = 0.5$ (red line), while the thermopower is less sensitive. The two vertical lines, signed with *o* and *s* mean the **stoichiometric** and optimized values of dimensionless Fermi energy.

From Figure 3 one can deduce that for stoichiometric crystals with $\varepsilon_F = 0.37$, $\sigma_{xx} = 10 \cdot 10^3 \Omega^{-1} cm^{-1}$ and $S_{xx} = 60\,\mu VK^{-1}$. When the concentration of conducting holes is diminished, the dimensionless Fermi energy decreases and for optimized crystals one can obtain high values of S_{xx}: $\varepsilon_F = 0.22$, $\sigma_{xx} = 5 \cdot 10^3\,\Omega^{-1} cm^{-1}$ and $S_{xx} = 120\,\mu VK^{-1}$. This can be explained in such manner: the less holes, the lower electrical conductivity but each hole carries more energy within the same temperature gradient.

In Figure 4 the electrical conductivity and electronic thermal conductivity are plotted as a function of dimensionless Fermi energy for the same temperature values.

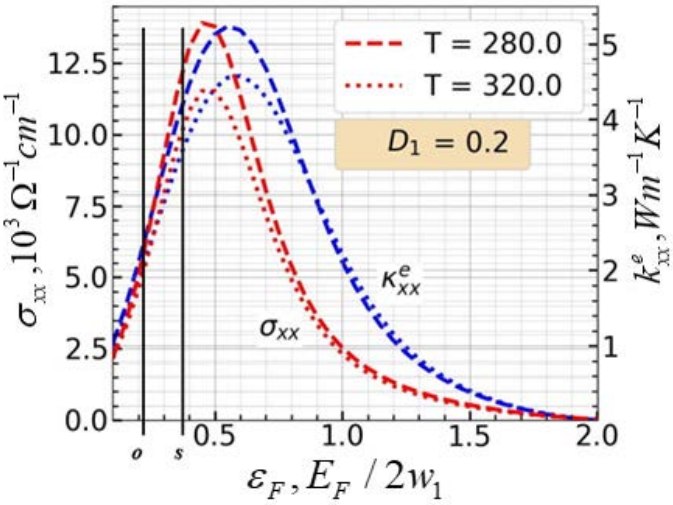

Figure 4. Electrical conductivity vs electronic thermal conductivity as a function of dimensionless Fermi energy. D_1 – scattering on lattice defects.

It can be observed that the manipulations with carrier concentration results in the creation of more lattice concentration. Also, with the increase of the temperature, the electrical conductivity and electronic thermal conductivity decreases. For *stoichiometric* values of dimensionless Fermi energy the following values were calculated: $\sigma_{xx} = 12 \cdot 10^3 - 10 \cdot 10^3\,\Omega^{-1}cm^{-1}$, $k^e_{xx} = 3.8 - 4\ Wm^{-1}K^{-1}$ for $T = 280\,K$ and $T = 320\,K$ respectively. For *optimized* crystals: $\sigma_{xx} = 5 \cdot 10^3\,\Omega^{-1}cm^{-1}$, $k^e_{xx} = 2.2\ Wm^{-1}K^{-1}$ and practically do not depend on *T*. The displacement of the maximums of σ_{xx} and k^e_{xx} indicate on the violation of the Wiedemann-Franz law in these crystals.

The obtained results are in accordance with the experimentally reported data, which indicates on the reliability of the physical model to perform numerical calculations and some predictions for a wider range of temperatures and carrier concentrations. It was shown that for such organic crystals, discussed above, a metallic-like electrical conductivity can be obtained with the tuning of charge carrier concentration. Also, due to the violation of the Wiedemann-Franz law, the electronic thermal conductivity increases slowly than the electrical conductivity when manipulating with carrier concentration. This phenomenon is very prospective for future thermoelectric applications. High values of thermopower, up to $120\ \mu VK^{-1}$, combined with low electronic thermal conductivity, $2.2\ Wm^{-1}K^{-1}$, is related to high thermoelectric figure-of merit that can be obtained in these crystals by evaporating iodine and lowering the Fermi level.

In what follows, we examine the characteristics of the Peierls transition in quasi-one-dimensional (Q1D) organic crystals of TTT_2I_3 [22]. The Peierls transition has been extensively investigated in the literature [23, 24]. In previous studies, its behavior has been explored in TTF–TCNQ crystals [25] as well as in TTT_2I_3 organic compounds [20, 22]. The objective of this work is to provide a comprehensive theoretical framework for the Peierls transition in TTT_2I_3 crystals, employing a three-dimensional physical model that simultaneously considers the two most relevant electron–phonon interaction mechanisms previously mention.

Figures 5 and 6 present the dependence of the renormalized phonon frequencies, $\Omega(q_x)$, on the wave-vector component q_x, for various temperatures, q_y and q_z values, and different Fermi quasi-momentum (k_F). Here, q_x, q_y and q_z denote the projections of the phonon quasi-wave vector along the *x*, *y*, and *z* directions, respectively.

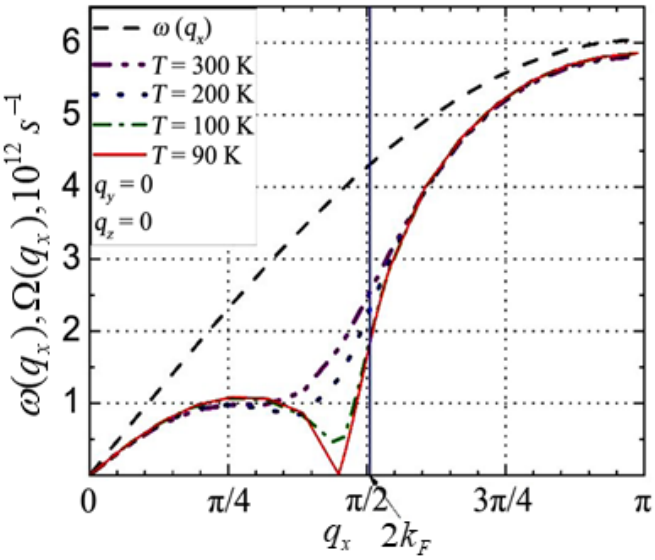

Figure 5. The renormalized phonon spectrum $\Omega(q_x)$ is plotted for several temperatures using $\gamma_1 = 1.7$, where the dashed curve represents the free-phonon spectrum [22]. The specific parameters used for this plot are $k_F = 0.502 \cdot \pi / 2$, $D = 1.057\, eV \cdot Å^{-1}$.

The initial (unrenormalized) phonon frequency is represented as $\omega(q_x)$, while (k_F) denotes the dimensionless Fermi quasi-momentum, determined by the carrier concentration. It is evident from all figures that $\Omega(q_x)$ exhibits lower values than $\omega(q_x)$ in the absence of electron–phonon coupling. This reduction reflects the softening of the lattice elastic constants due to electron–phonon interactions. Additionally, decreasing the temperature *T* leads to a noticeable change in the shape of the curves. A minimum develops in the $\Omega(q_x)$ dependence, becoming increasingly pronounced at lower temperatures. The expected behavior was that $\Omega(q_x)$ would vanish at $q_x = 2k_F$ at a certain critical temperature, indicating the occurrence of the Peierls structural transition.

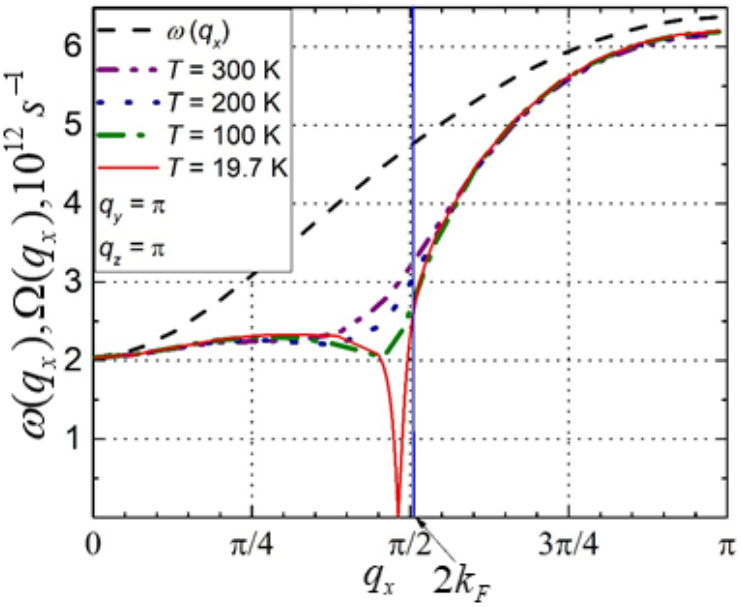

Figure 6. The renormalized phonon spectrum Ω(qₓ) is plotted for several temperatures using $\gamma_1 = 1.7$, where the dashed curve represents the free-phonon spectrum [22]. The specific parameters used for this plot are $k_F = 0.502 \cdot \pi / 2$, $D = 1.055\, eV \cdot Å^{-1}$.

However, our calculations show that the renormalized phonon frequency reaches zero at a value $q_x \neq 2k_F$. This discrepancy arises from the deviation of k_F from π/4. Figure 5 represents the case where $q_y = 0$ and $q_z = 0$, with the dimensionless Fermi momentum $k_F = 0.502 \cdot \pi / 2$. The parameter *D* is set to $1.057 eV \cdot Å^{-1}$, and the interaction between TTT chains is neglected. In this scenario, the Peierls transition begins at $T = 90 K$, at which point the electrical conductivity reaches its maximum. As the temperature decreases, the electrical conductivity gradually diminishes. This transition temperature value is very close to that presented in the experimental curve in [16].

Figure 6 corresponds to the case where the interaction between TTT chains is included $(q_y = \pi, q_z = \pi)$, with $D = 1.055 eV \cdot Å^{-1}$ and $k_F = 0.502 \cdot \pi / 2$. As shown in the figure, the transition is completed at $T = 19.7 K$. It is evident from Figure 1 that the electrical conductivity drops sharply and approaches zero at approximately *T ~ 20 K*. Furthermore, it is observed that the parameter *D* decreases, indicating a weaker interaction between holes and defects in this case. Also, it was observed that the interchain interaction, reduces the transition temperature. The interactions between holes and phonons, as well as those with structural defects, lead to a reduction in $\Omega(q_x)$ and a decrease in the sound velocity over a wide temperature range.

4. Conclusions

A more complete physical model for nanostructured organic crystals of tetratiotetracene-iodide was developed and applied for numerical calculations of electrical conductivity, electronic thermal conductivity and thermopower (Seebeck coefficient). The calculations were performed for a range of temperatures from $20 K$ to $400 K$, revealing a strange behavior near $T = 90 K$, explained by the metal-dielectric transition of the Peierls type. For temperatures near to $300 K$, the physical model is completely applicable for calculating the thermoelectric properties of the crystal. It was demonstrated by numerical calculations that when manipulating with charge carrier concentration, which leads to the variation of the Fermi level, the thermopower can be increased significantly, with a slow diminution in electrical conductivity. Moreover, the thermal conductivity carried by electrons decreases also, which indicates that in such materials a high value of thermoelectric figure-of-merit can be obtained.

Acknowledgments: This work was funded by Ministry of Education and Research from the Republic of Moldova (institutional subprogram #02.04.02) "Development of technologies and investigation of the properties of layered semiconductor compounds, hybrid nanostructures and laser sources."

Conflicts of Interest: The authors declare no conflict of interest.

References

1. Venkatasubramanian, R.; Sivola, E.; Colpitts, T.; O'Quinn, B. Thin-Film Thermoelectric Devices with High Room- Temperature Figure of Merit. *Nature* 2001, 413, pp. 597-602.
2. Dresselhaus, M.S.; Heremans, J.P. Thermoelectric Handbook: Macro to Nano. CRC Press, Boca Raton, 2006, 49, 16 p.
3. Vining, C.B. ZT~3.5: Fifteen Years Progress and Things to Come. In: *The Proceedings of the 5th European Conference on Thermoelectrics*, Eindhoven, 18-22 May 2008, pp. 5-10.
4. Harman, T.C.; Walsh, M.P.; Laforge, B.E; Turner, G.W. Nanostructured Thermoelectric Materials. *Journal of Electronic Materials* 2005, 34, L19-L22.

5.Transmission Lasers (DWDM). Available online: http://www.marlow.com/industries/telecommunications/transmission-lasers-dwdm.html (accessed on 02.09.2025).
6. Climate Seats. Available online: https://gentherm.com/en/ (accessed on 02.09.2025).
7. Global Leader in Thermoelectric Products. Available online: https://www.koolatron.com/ (accessed on 02.09.2025).
8. He, R.; Schierning, G.; Nielsch, K. Thermoelectric Devices: A Review of Devices, Architectures, and Contact Optimization. *Advanced Materials Technologies* 2018, 3, 1700256.
9. Siouane, S.; Jovanovic, S.; Poure, P. Fully Electrical Modeling of Thermoelectric Generators with Contact Thermal Resistance under Different Operating Conditions. *Journal of Electronic Materials* 2017, 46, pp. 40-50.
10. Shi, Y.; Sturm, C.; Kleinke, H. Chalcogenides as Thermoelectric Materials. *Journal of Solid State Chemistry* 2019, 270, pp. 273-279.
11. d'Angelo, M.; Galassi, C.; Lecis, N. Thermoelectric Materials and Applications: A Review. *Energies* 2023, 16, 6409.
12. Kim, G.H.; Shao, L.; Zhang, K.; Pipe, K.P. Engineered Doping of Organic Semiconductors for Enhanced Thermoelectric Efficiency. *Nature Materials* 2013, 12, pp. 719- 723.
13. Taroni, J.; Hoces I.; Stingelin, N.; Heeney, M; Bilotti, E. Thermoelectric Materials: A Brief Historical Survey from Metal Junctions and Inorganic Semiconductors to Organic Polymers. *Israel Journal of Chemistry* 2014, 54, pp. 534-552.
14. Casian, A.; Pflaum, J.; Sanduleac, I. Prospects of Low Dimensional Organic Materials for Thermoelectric Applications. *Journal of Thermoelectricity* 2015, 1, pp. 16-26.
15. Sanduleac, I.; Casian, A. Nanostructured TTT(TCNQ)2 Organic Crystals as Promising Thermoelectric n-Type Materials: 3D Modeling. *Journal of Electronic Materials* 2015, 45, pp. 1316-1320.
16. Kaminskii, V.F.; Khidekel', M.L. Lyubovskii, R.B. et all. Metal-Insulator phase transition in TTT2I3 affected by iodine concentration. *Phys. Status Solidi A*, 1977, 44, 77.
17. Casian, A. Sanduleac, I. Thermoelectric Properties of Tetrathiotetracene Iodide Crystals: Modeling and Experiment, *J. Electron. Mat.* 2014, 43, 3740.
18. Casian, A.; Dusciac, V.; Nicic, V. Thermoelectric Opportunities of Quasi-One-Dimensional Organic Crystals of Tetrathiotetracene–Iodide. *J. Thermoelectricity* 2009, 2, pp. 33-39.
19. Casian, A.; Stockholm, J.; Dusciac, V.; Nicik, V. Low-Dimensional Organic Crystal Tetrathiotetracene–Iodide as Thermoelectric Material: Reality and Prospects. *J. Nanoelectronics and Optoelectronics* 2009, 4, pp. 95-100.
20. Andronic, S.; Casian, A. Metal-Insulator Transition of Peierls Type in Quasi-One-Dimensional Crystals of TTT_2I_3. *Advances in Materials Physics and Chemistry* 2017, 7, pp. 212-222.
21. Graja, A. *Low-Dimensional Organic Conductors*. Word Scientific, Singapore, 1989, 306 p.
22. Andronic, S.; Casian, A. Peierls Structural Transition in Q1D Organic Crystals of TTT2I3 for Different Values of Carrier Concentration. *Advances in Materials Physics and Chemistry* 2020, 10, pp. 239-251.
23. Bulaevskii, L.N. Peierls Structure Transition in Quasi-One-Dimensional Crystals. *Soviet Physics Uspekhi* 1975, 18, pp. 131-150.
24. Hohenadler, M.; Fehske, H.; Assaad, F.F. Dynamic Charge Correlations near the Peierls Transition. *Physical Review B* 2011, 83, 115105.
25. Andronic, S.; Casian, A. Phonons near Peierls Structural Transition in Quasi-One-Dimensional Organic Crystals of TTF-TCNQ. *Advances in Materials Physics and Chemistry* 2016, 6, pp. 98-104.

Citation: Andronic, S.; Sanduleac, I. TTT_2I_3 organic crystals – a promising platform for low-dimensional thermoelectric devices. *Journal of Engineering Science*. 2025, XXXII (4), pp. 7-18. https://doi.org/10.52326/jes.utm.2025.32(4).01.

Submission of manuscripts: jes@meridian.utm.md